MIKAILALSYS
Journal of Multidisciplinary Sciences

e-ISSN : 2987-2286
p-ISSN : 2987-3924
Index: Harvard, Boston, Sydney, Copernicus, Sinta 4, Scilit, Semantic, Google, etc

https://doi.org/10.58578/mikailalsys.v4i3.12504

Stability Analysis and Optimal Xylitol Harvesting by *Debaryomyces hansenii* on OPEFB Hydrolysate

Alvioni Bani & Nur Rahmah Yunita Abar
Universitas Negeri Makassar, Indonesia
alvioni.bani@unm.ac.id

Submitted:	Revised:	Accepted:	Published:
Sep 20, 2026	Oct 19, 2026	Oct 30, 2026	Nov 4, 2026

Abstract

Although xylitol fermentation from lignocellulosic hydrolysates has received considerable modeling attention, optimal harvesting timing and duration remain insufficiently explored. This study determined the optimal harvesting schedule for xylitol produced by *Debaryomyces hansenii* from oil palm empty fruit bunch (OPEFB) hydrolysate using mathematical analysis and numerical simulation. An existing fourteen-metabolite model was reduced to a three-dimensional xylose–xylitol–xylulose cascade using kinetic parameters from the original model. The reduced system was examined through equilibrium and stability analysis, while the peak time and width of a Gaussian harvesting window were optimized using grid search and Nelder–Mead optimization in MATLAB. The reduction preserved the full model's steady state exactly, and the analysis established a unique, globally stable positive equilibrium under active harvesting. With the window width adopted in the earlier model, advancing the harvesting peak from 72 h to approximately 17 h increased harvested xylitol by 66.9%. Under the parameter perturbations examined, optimal peak times ranged from 34 to 44 h. Even continuous harvesting recovered less than 20% of the supplied precursor, with oxidation by xylitol dehydrogenase limiting recovery. These findings demonstrate the value of reduced metabolic models for bioprocess optimization and identify harvesting timing as an important determinant of predicted xylitol recovery. The study provides model-based scheduling guidance that complements enzyme-level strategies, while highlighting the need to incorporate biomass growth and experimentally validate the proposed harvesting schedules.

Mikailalsys is licensed under a Creative Commons Attribution-NonCommercial-ShareAlike 4.0 International License

Keywords: *Debaryomyces hansenii*; Xylitol; Optimal Harvesting; Metabolic Model Reduction; Stability Analysis

INTRODUCTION

Two of the most widespread chronic conditions in the world are tied to sugar consumption. An estimated 589 million adults aged 20-79 years were living with diabetes in 2024 (International Diabetes Federation, 2025), while oral diseases affect close to 3.5 billion people, with untreated dental caries being the single most common condition (World Health Organization, 2022). Xylitol speaks to both problems. It raises blood glucose much less than sucrose (Gasmi Benahmed et al., 2020), and regular use of xylitol chewing gum has been associated with lower levels of mutans streptococci and reduced plaque accumulation (Söderling & Pienihäkkinen, 2025). Indonesia produces very little xylitol of its own, even though it has one of the largest potential feedstocks for it. Suhartini et al. (2022) estimated that the hemicellulose in Indonesian oil palm empty fruit bunches (OPEFB), if processed together with bioethanol, could yield about 7.7 thousand tonnes of xylitol per year. Turning that estimate into actual product has proven difficult. In fermentation trials on OPEFB hydrolysate, *Debaryomyces hansenii* reached a maximum xylitol concentration of only 2.86 g/L, corresponding to 0.297 g of xylitol per gram of xylose (Mardawati et al., 2022). The bottleneck, in other words, is no longer the availability of raw material but the efficiency with which xylose ends up as recoverable xylitol.

Part of the explanation lies inside the cell. In *D. hansenii*, xylose reductase converts xylose to xylitol, but xylitol dehydrogenase then oxidizes part of that xylitol to xylulose, which is channeled into the pentose phosphate pathway (Navarrete et al., 2022). Xylitol is therefore an intermediate that the cell keeps consuming, not a final product it simply accumulates. Experimental work has responded mostly at the genetic level, by modifying xylitol dehydrogenase in *D. hansenii* (Biswas et al., 2013; Pal et al., 2013) or by disrupting its gene in other xylose-fermenting yeasts (Ko et al., 2006). We take a different view. If xylitol is continuously drained by an enzyme, then the moment at which it is removed from the system, and the length of time over which removal takes place, should matter as much as the rate at which it is formed. This is an operational choice that requires no strain engineering. A mass balance on the steady state of our earlier metabolic model (Bani et al., 2025) shows why the choice matters. With a steady-state xylitol concentration of 0.519 mM and a

harvesting rate constant of 0.38 h^{-1}, only about 0.20 mM h^{-1} of the 1.0 mM h^{-1} entering the xylitol pool is harvested, and the remaining 80% is lost to oxidation. Even a modest improvement in how the harvest is scheduled could therefore change the amount of xylitol recovered noticeably.

Mathematical models of xylitol fermentation have developed along two lines. The first consists of unstructured models that track biomass, substrate, and product at the level of the culture. Kasbawati et al. (2022) compared the Aiba, Monod, Ghose, and Tyagi growth kinetics for *D. hansenii* on OPEFB hydrolysate. Manjarres-Pinzón et al. (2021) fitted the Monod, Contois, and Tessier models to *Candida tropicalis* grown in synthetic medium and in non-detoxified OPEFB hydrolysate. Feng et al. (2024) proposed a co-substrate model with substrate and product inhibition for xylose–glucose mixtures and validated it on corncob hydrolysate, and Bani et al. (2026) found that Moser kinetics with non-growth-associated product formation best described the *D. hansenii* data. These models reproduce concentration profiles well, but they say nothing about where the xylitol goes inside the cell, so they cannot be used to study the competition between harvesting and xylitol dehydrogenase. The second line consists of structured models that follow intracellular metabolites explicitly (Kasbawati et al., 2018, 2020). Our fourteen-metabolite model of *D. hansenii* (Bani et al., 2025) belongs to this group and introduced a Gaussian harvesting function, $h(t,\beta) = \delta_1 S_5(t), e^{-\beta(t-t_h)^2}$, where t_h is the time of peak harvesting and β controls the width of the harvesting window. In that study, however, both quantities were fixed in advance ($t_h = 72\,h$ dan $\beta = 1/t_f$) rather than optimized. Because of the size of the system, several steady-state concentrations were also available only numerically, and stability was judged from numerically evaluated eigenvalues. To our knowledge, no study has yet treated the timing and duration of xylitol harvesting as decision variables, and none has offered a model small enough for this question to be answered analytically.

This study fills that gap in two steps. First, we show that the harvesting question involves only the upstream part of the network. Glycolysis and the ethanol branch draw flux from xylitol but return none to it, so the fourteen-metabolite system can be reduced to a three-dimensional cascade of xylose, xylitol, and xylulose without altering the xylitol dynamics. For this reduced model the equilibrium can be written in closed form. We prove that a unique positive xylitol equilibrium exists whenever harvesting is active and that it is asymptotically stable. The reduced model reproduces exactly the xylose, xylitol, and xylulose

steady states reported by Bani et al. (2025), which indicates that the reduction preserves the relevant behavior. Second, we treat the harvesting time t_h and the window parameter β as decision variables and search for the pair that maximizes harvested xylitol after accounting for the cost of keeping the harvesting window open. The analysis is grounded in Michaelis–Menten enzyme kinetics, mass-balance formulation of metabolite dynamics, the quasi-steady-state approximation for the polymeric substrates, and linearized stability theory (Perko, 2001). The harvesting formulation follows the trade-off, standard in bioeconomic harvesting models, between the yield obtained and the effort spent to obtain it (Clark, 2010).

Accordingly, this study focuses on the harvesting stage of xylitol production by *D. hansenii* from OPEFB hydrolysate, examined through a reduced metabolic model. It aims to derive the reduced three-dimensional model from the earlier fourteen-metabolite framework, to establish the existence, uniqueness, and stability of its positive equilibrium, and to determine the harvesting time and window width that give the largest net amount of harvested xylitol. Through these results, the study seeks to offer a practical, model-based guideline for scheduling xylitol recovery that complements the enzyme-level strategies identified in our previous work.

METHODS

This study is a theoretical quantitative investigation based on mathematical modeling and numerical simulation. No new laboratory measurements were made. The work proceeded in four stages. First, a reduced model was derived from the fourteen-metabolite model of Bani et al. (2025). Second, an autonomous reference version of this model was analyzed to establish positivity, equilibrium, and stability. Third, a harvesting optimization problem was formulated on the full non-autonomous model. Fourth, the problem was solved numerically, and the robustness of the solution was assessed. The analytical stage ensures that the numerical experiments are performed on a well-posed system. The numerical stage answers the optimization question, which has no closed-form solution.

Model Reduction

The parent model of Bani et al. (2025) describes fourteen intracellular metabolites of *Debaryomyces hansenii* linked by fourteen enzymatic reactions. To isolate the part of the network that governs xylitol (S_5), we traced the direction of flux through the network. First,

Downstream reactions were removed**.** Reactions from xylulose-5-phosphate onward, covering the pentose phosphate pathway, glycolysis, and the ethanol and acetate branches, receive carbon from xylitol but return none to it. They can therefore be removed without changing the xylitol dynamics. Second, Polymeric substrates and glucose were placed under the quasi-steady-state approximation**.** Hemicellulose and cellulose are converted rapidly compared with the slower release of lignocellulose, so their dynamics were replaced by the release rate itself (Segel & Slemrod, 1989). Glucose was treated in the same way, so its conversion to xylitol by glucose isomerase enters the model as an inflow equal to the cellulose-derived release rate. Lignocellulose is consumed during batch operation and follows $dL/dt = -\alpha L$ with $L(0) = L_0$. The inflows of xylose and of glucose-derived xylitol are then

$$F(t) = p\alpha L_0 e^{-\alpha t}, G(t) = (1-p)\alpha L_0 e^{-\alpha t}.$$

The reduced model is

$$\begin{aligned} \frac{dS_3}{dt} &= F(t) - \frac{V_3 S_3}{K_3 + S_3}, \\ \frac{dS_5}{dt} &= \frac{V_3 S_3}{K_3 + S_3} + G(t) - \frac{V_5 S_5}{K_5 + S_5} - h(t,\beta), \\ \frac{dS_6}{dt} &= \frac{V_5 S_5}{K_5 + S_5} - \frac{V_6 S_6}{K_6 + S_6}. \end{aligned} \tag{1}$$

where S_3, S_5, and S_6 are the concentrations (mM) of xylose, xylitol, and xylulose. All reactions follow irreversible Michaelis-Menten kinetics, as in the parent model. Xylitol is removed through the harvesting function:

$$h(t,\beta) = \delta_1 S_5(t) e^{\beta (t - t_h)^2} \tag{2}$$

where t_h (h) is the time of peak harvesting and β (h^{-2}) sets the width of the harvesting window. Smaller β gives a wider window. In the limit $\beta \to 0$, harvesting proceeds at the constant maximum rate $\delta_1 S_5$. To keep track of where xylitol ends up, two cumulative quantities were appended:

$$\frac{dH}{dt} = h(t,\beta), \frac{dZ}{dt} = \frac{V_5 S_5}{K_5 + S_5}, H(0) = Z(0) = 0, \tag{3}$$

So that $H(t)$ is the total xylitol harvested and $Z(t)$ the total exidized by xilitol dehydrogenase. Neithe wuality feeds back into system (1).

All parameters are assumed to be positive. The analytical results in Section 3.1 hold for any positive parameter values. For the numerical solution, the kinetic parameters retained

after the reduction were taken unchanged from the parent model of Bani et al. (2025), so that the reduced model can be checked directly against the published steady state and so that differences in outcome can be attributed to the harvesting schedule alone. The values used are listed in Section 3.2.

Formulation of the Harvesting Problem

A harvesting schedule is determined by the pair (t_h, β), in which t_h fixes the moment at which harvesting reaches its peak and β governs how long the harvest lasts. To compare different schedules, we first consider the total amount of xylitol collected during the fermentation, $H(t_f)$, which follows directly from Equation (3). This quantity, however, says nothing about how long the harvesting operation has to be kept running in order to collect that amount. Since the window in Equation (2) has a Gaussian shape in time, its duration can be summarized by the area under the window profile, which defines the effective window width

$$W(\beta) = \int_{-\infty}^{\infty} e^{-\beta(t-t_h)^2} dt = \sqrt{\pi/\beta}\,. \tag{4}$$

A small value of β therefore corresponds to a long harvest spread over much of the fermentation, whereas a large value concentrates the harvest in a short interval around t_h. To judge how well a schedule uses the available substrate, the harvest is also compared with the total amount of xylitol precursor supplied to the cell during the run, giving the harvesting efficiency

$$\eta(t_h, \beta) = \frac{H(t_f)}{\int_0^{t_f}\big(F(t) + G(t)\big)dt} \times 100\% = \frac{H(t_f)}{L_0(1 - e^{-\alpha t_f})} \times 100\%, \tag{5}$$

where the denominator takes a closed form because $F(t) + G(t) = \alpha L_0 e^{-\alpha t}$. The efficiency thus expresses the fraction of the released substrate that is recovered as harvested xylitol instead of being oxidized by xylitol dehydrogenase.

Choosing a schedule simply by maximizing H would not lead to a useful answer. A wider window always collects more xylitol, so the optimum would be reached as $\beta \to 0$, which amounts to harvesting continuously from the beginning to the end of the fermentation. In practice, keeping a harvesting operation running is not free, since it requires energy and separation effort and may disturb the culture. For this reason we adopt the trade-off between yield and effort that underlies bioeconomic harvesting models (Clark, 2010) and

define the net benefit of a schedule as the amount harvested minus a cost that grows with the width of the window. The harvesting problem then reads:

$$\max_{(t_h,\beta)\in\Omega} J(t_h,\beta) = H\big(t_f : t_h,\beta\big) - c_\omega\sqrt{\pi/\beta}, \qquad \Omega = \big[0, t_f\big] \times [\beta_{min}, \beta_{max}], \tag{6}$$

subject to the dynamics (1)–(3), where c_ω $(mM\ h^{-1})$ denotes the cost per unit of window width. Both terms of J are expressed in mM, so the objective is dimensionally consistent. When $c_\omega = 0$ the problem reduces to maximizing the harvest, and as c_ω increases the optimal window becomes progressively narrower. Since no reported value of c_ω is available for this system, several scenario values are examined so that the conclusions do not depend on a single arbitrary choice.

All computations were carried out in MATLAB R2015a. The equilibrium and the Jacobian matrix of the reference model were derived with the Symbolic Math Toolbox and checked against a central finite-difference approximation. Because the eigenvalues of the reference model differ by more than two orders of magnitude, system (1)–(3) is mildly stiff. It was therefore integrated with the solver ode15s (Shampine & Reichelt, 1997), using a relative tolerance of 10^{-8} and an absolute tolerance of 10^{-10}, and selected runs were repeated with ode45 to confirm the solutions. Before the optimization was carried out, the reduced model was verified in two ways: its equilibrium was compared with the steady state reported for the full model, and its simulated trajectories were checked for convergence to that equilibrium.

RESULTS

Mathematical Analysis

The analysis begins with the reference model introduced in Section 2.1, in which the inflows are held at their initial values, $F = p\alpha L_0$ and $G = (1-p)\alpha L_0$, and harvesting acts at the constant maximum rate $\delta_1 S_5$. Writing $\varphi_i(S_i) = V_i S_i/(K_i + S_i)$ for the Michaelis-Menten rate functions, with $i = 3, 5, 6$, the reference model reads

$$\begin{aligned}
\frac{dS_3}{dt} &= F(t) - \varphi_3(S_3),\\
\frac{dS_5}{dt} &= \varphi_3(S_3) + G - \varphi_5(S_5) - \delta_1 S_5,\\
\frac{dS_6}{dt} &= \varphi_5(S_5) - \varphi_6(S_6).
\end{aligned} \tag{7}$$

Each φ_i is strictly increasing on $[0, \infty)$, vanishes at zero, and is bounded above by V_i. The system has a cascade structure i.e. S_3 evolves independently, S_5 depends only on S_3, and S_6 depends only on S_5. Before analyzing its equilibrium, we establish that the original non-autonomous model (1) is well posed.

Lemma 1. *For any non-negative initial condition, the solution of system (1) remains non-negative and bounded for all $t \geq 0$, and*

$$S_3(t) + S_5(t) + S_6(t) \leq S_3(0) + S_5(0) + S_6(0) + L_0(1 - e^{-\alpha t}). \quad (8)$$

Proof. The right-hand side of system (1) is continuously differentiable, so a unique local solution exists. On the face $S_3 = 0$ of the non-negative orthant, $\frac{dS_3}{dt} = F(t) > 0$. On the face $S_5 = 0$, the oxidation and harvesting terms both vanish, so $\frac{dS_5}{dt} = \varphi_3(S_3) + G(t) \geq 0$. On the face $S_6 = 0$, $\frac{dS_6}{dt} = \varphi_5(S_5) \geq 0$. The vector field therefore never points out of the orthant, and solutions starting in it remain there. Adding the three equations gives $\frac{d(S_3 + S_5 + S_6)}{dt} = F(t) + G(t) - h(t, \beta) - \varphi_6(S_6) \leq \alpha L_0 e^{-\alpha t}$, since h and φ_6 are non-negative. Integrating over $[0, t]$ yields (8). Since every variable is non-negative and their sum is bounded, every variable is bounded, and the solution extends to all $t \geq 0$.

Setting the right-hand sides of (7) to zero and solving along the cascade, the first equation requires $\varphi_3(S_3) = F$, which has a positive solution if and only if $F < V_3$:

$$S_3^* = \frac{FK_3}{V_3 - F}. \quad (9)$$

The xylose reductase flux then equals F, so the second equation becomes $Q - \varphi_5(S_5) - \delta_1 S_5 = 0$ with $Q = F + G = \alpha L_0$. Multiplying by $K_5 + S_5$ gives:

$$\delta_1 S_5^2 + (V_5 + \delta_1 K_5 - Q) S_5 - Q K_5 = 0, \quad (10)$$

whose leading coefficient is positive and whose constant term is negative. By Descartes' rule of signs, equation (10) has exactly one positive root:

$$S_5^* = -\frac{(V_5 + \delta_1 K_5 - Q) + \sqrt{(V_5 + \delta_1 K_5 - Q)^2 + 4\delta_1 Q K_5}}{2\delta_1}. \quad (11)$$

Denoting by $R = \varphi_5(S_5^*) = Q - \delta_1 S_5^*$ the equilibrium flux through xylitol dehydrogenase, so that $0 < R < Q$, the third equation has a positive solution if and only if $R < V_6$:

$$S_6^* = \frac{RK_6}{V_6 - R}. \tag{12}$$

Theorem 1. *The reference model (7) has a positive equilibrium* $E* = (S_3*, S_5*, S_6*)$ *if and only if* $F < V_3$ *and* $R < V_6$. *In that case, the equilibrium is unique and given by (9), (11), and (12). A sufficient condition is* $F < V_3$ *and* $\alpha L_0 < V_6$.

Proof. The sufficient condition follows from $R < Q = \alpha L_0$. Without harvesting $(\delta_1 = 0)$, equation (10) reduces to a linear equation with solution $S_5^* = QK_5/(V_5 - Q)$, which is positive only if $Q < V_5$. With $\delta_1 > 0$, by contrast, the xylitol equilibrium exists for all positive parameter values.

The Jacobian matrix of (7) at E^* is

$$J(E^*) = \begin{pmatrix} -a & 0 & 0 \\ a & -(b+\delta_1) & 0 \\ 0 & b & -c \end{pmatrix}, \tag{13}$$

$a = \frac{V_3K_3}{(K_3+S_3^*)^2}, b = \frac{V_5K_5}{(K_5+S_5^*)^2}, c = \frac{V_6K_6}{(K_6+S_6^*)^2}$, or $a = \varphi_3'(S_3^*), b = \varphi_5'(S_5^*)$, and $c = \varphi_6'(S_6^*)$. Since the matrix is lower triangular, its eigenvalues lie on the diagonal.

Theorem 2. *Whenever* E^* *exists, it is locally asymptotically stable, with real negative eigenvalues* $\lambda_1 = -a, \lambda_2 = -(b + \delta_1)$, *and* $\lambda_3 = -c$.

Proof. All parameters are positive, so $a, b, c > 0$ and $\delta_1 > 0$. The three eigenvalues are therefore real and negative, and the conclusion follows from the linearization theorem (Perko, 2001).

Theorem 3. *If* $F < V_3$ *and* $R < V_6$, *every solution of (7) starting in the non-negative orthant converges to* E^* *as* $t \to \infty$.

Proof. The right-hand side of the first equation, $F - \varphi_3(S_3)$, is strictly decreasing in S_3 and vanishes only at S_3^*, so $S_3(t)$ converges monotonically to S_3*. The second equation can be written as $\frac{dS_5}{dt} = g(S_5) + \varepsilon(t)$, where $g(S_5) = Q - \varphi_5(S_5) - \delta_1 S_5$ is strictly decreasing with unique zero S_5^*, and $\varepsilon(t) = \varphi_3(S_3(t)) - F$ tends to zero. For any $\kappa > 0$ there is a time T beyond which $|\varepsilon(t)| < \kappa$. From then on, by the comparison principle, S_5 lies between the solutions of $\frac{dS_5}{dt} = g(S_5) \mp \kappa$. The equilibria of these two equations converge to S_5^* as $\kappa \to 0$, so $S_5(t) \to S_5^*$, consistent with the theory of asymptotically

autonomous equations (Thieme, 1992). The same argument applied to the third equation, with $g(S_6) = R - \varphi_6(S_6)$, gives $S_6(t) \to S_6^*$.

At equilibrium, the inflow Q into the xylitol pool divides between oxidation at rate R and harvesting at rate $\delta_1 S_5^*$, so the fraction recovered by harvesting is

$$\theta^* = \frac{\delta_1 S_5^*}{Q} = 1 - \frac{R}{Q}. \quad (14)$$

Proposition 1. *The equilibrium concentration S_5^* decreases as δ_1 or V_5 increases. The harvested fraction θ^* increases with δ_1 and decreases with V_5.*

Proof. S_5^* is defined implicitly by $\Psi(S_5, \delta_1, V_5) = \varphi_5(S_5) + \delta_1 S_5 - Q = 0$, with $\frac{\partial \Psi}{\partial S_5} = \varphi_5'(S_5) + \delta_1 > 0$. The implicit function theorem gives

$$\frac{\partial S_5^*}{\partial \delta_1} = -\frac{S_5^*}{\varphi_5'(S_5^*) + \delta_1} < 0, \frac{\partial S_5^*}{\partial V_5} = -\frac{\frac{S_5^*}{K_5 + S_5^*}}{\varphi_5'(S_5^*) + \delta_1} < 0.$$

Since $\theta^* = 1 - \varphi_5(S_5^*)/Q$ and φ_5 is increasing, the decrease of S_5^* with δ_1 raises θ^*. Since $\theta^* = \delta_1 S_5^*/Q$ is proportional to S_5^* for fixed δ_1, it decreases with V_5.

These results hold for any positive parameter values. In the next subsection, they are quantified using the parameters of the parent model, and the reduced model is used to solve the harvesting problem (6).

Numerical Solutions

To illustrate the analytical results and to solve the harvesting problem, the reduced model was simulated with the parameter values in Table 1. All kinetic parameters were taken from the parent model (Bani et al., 2025), where their original sources are documented. The fermentation was assumed to start with no intracellular xylose, xylitol, or xylulose, so that $S_3(0) = S_5(0) = S_6(0) = 0$.

Table 1. Parameters of the reduced model.

Parameter	Description	Value	Unit	Source
α	Inlet rate of lignocellulose	0.01	h^{-1}	Bani et al. (2025)
L_0	Initial lignocellulose concentration	100	mM	Bani et al. (2025)

p	Fraction released as hemicellulose	0.4	-	Bani et al. (2025)
V_3	Maximum rate of xylose reductase	22.3	$\mathrm{mMh^{-1}}$	Bani et al. (2025)
K_3	Michaelis constant of xylose reductase	80	mM	Bani et al. (2025)
V_5	Maximum rate of xylitol dehydrogenase	98.6	$\mathrm{mMh^{-1}}$	Bani et al. (2025)
K_5	Michaelis constant of xylitol dehydrogenase	63.3	mM	Bani et al. (2025)
V_6	Maximum rate of xylulokinase	32.4	$\mathrm{mMh^{-1}}$	Bani et al. (2025)
K_6	Michaelis constant of xylulokinase	0.25	mM	Bani et al. (2025)
δ_1	Maximum harvesting rate constant	0.38	$\mathrm{h^{-1}}$	Bani et al. (2025)
t_f	Fermentation horizon	100	h	Bani et al. (2025)
t_h	Time of peak harvesting	decision variable	h	This study
β	Width parameter of the harvesting window	decision variable	$\mathrm{h^{-2}}$	This study
c_ω	Cost per unit of window width	scenario values	$\mathrm{mMh^{-1}}$	This study

With the parameter values in Table 1, both conditions of Theorem 1 are satisfied by a wide margin. The xylose supply $F = 0.4\,mM\,h^{-1}$ is far below the capacity of xylose reductase, $V_3 = 22.3\,mM\,h^{-1}$, and the total inflow $\alpha L_0 = 1\,mM\,h^{-1}$ is far below the capacity of xylulokinase, $V_6 = 32.4\,mM\,h^{-1}$. The closed-form expressions (9), (11), and (12) give the equilibrium of the reference model as $S_3^* = 1.46119\,mM, S_5^* = 0.51949\,mM$, and $S_6^* = 0.00635\,mM$. These values coincide with the steady state of the corresponding metabolites in the fourteen-metabolite model, reported as $1.46118, 0.51948,$ and $0.00635\,mM$ (Bani et al., 2025). The reduction therefore preserves the behavior of the xylitol pool exactly, not merely approximately. The eigenvalues of the Jacobian (13) at this equilibrium are $\lambda_1 = -0.2688\,h^{-1}, \lambda_2 = -1.9124\,h^{-1},$ and $\lambda_3 = -123.26\,h^{-1}$, all real and negative as Theorem 2 requires. Integrating the reference model from an empty initial pool confirmed that the solution converges to this equilibrium, in agreement with Theorem 3. At the equilibrium, the harvested fraction defined in (14) is $\theta^* = 19.74\%$. In other words, even

under continuous harvesting at the maximum rate, about 80% of the xylitol entering the pool is oxidized by xylitol dehydrogenase.

The eigenvalues also separate the time scales of the batch model. The slowest intracellular relaxation time is $1/|\lambda_1| = 3.72$ h, whereas the supply of lignocellulose-derived sugar decays on the time scale $1/\alpha = 100$ h. Figure 1 shows the consequence of this separation. Without harvesting, xylitol rises quickly to a peak of 0.578 mM at about 9.9 h and then declines slowly as the supply decreases. Under continuous harvesting, the peak is lower, 0.463 mM at 9.7 h, and beyond this point the trajectory stays within about *2%* of the quasi-equilibrium obtained from (11) with Q replaced by $\alpha L_0 e^{-\alpha t}$. Harvesting has no effect on xylose because the cascade transmits no influence upstream. Over the 100 h of fermentation, the cell receives a total of 63.21 mM of xylitol precursor. Without harvesting, 62.42 mM of it is oxidized to xylulose. With continuous harvesting, 12.30 mM is recovered and 50.16 mM is oxidized, giving an efficiency of $\eta = 19.47\%$. This value is close to the equilibrium fraction θ^*, as expected from the quasi-equilibrium behavior, and it represents the upper bound on what any harvesting schedule can achieve with these parameters.

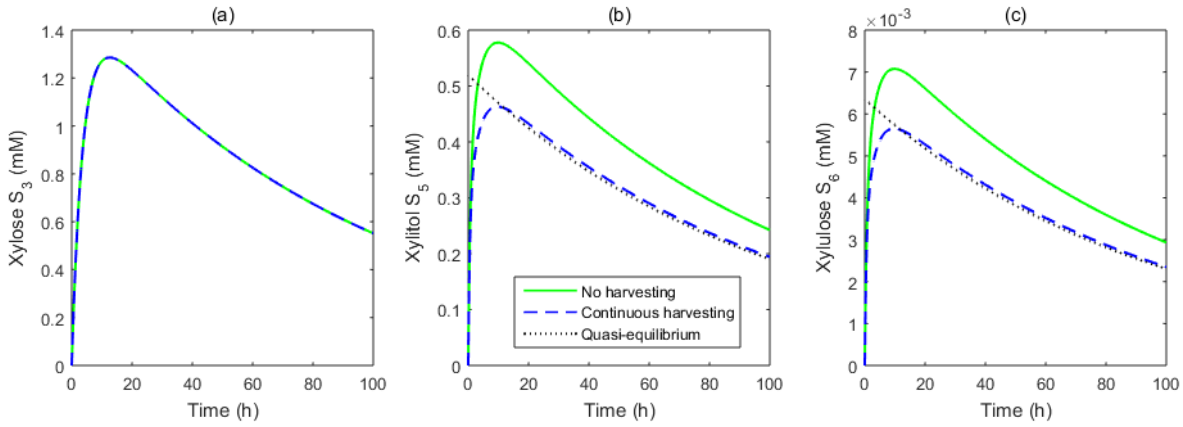


Figure 1. Dynamics of (a) xylose, (b) xylitol, and (c) xylulose in the batch model without harvesting (solid green) and with continuous harvesting at the maximum rate (dashed blue). The dotted line shows the quasi-equilibrium obtained from (11) and (12) with Q replaced by $\alpha L_0 e^{-\alpha t}$.

The timing of the harvesting window has a large effect on the amount collected. Figure 2 shows the cumulative harvest $H(t_f)$ as a function of the peak time t_h for four fixed window widths. For every width, $H(t_f)$ ia a unimodal function of t_h with a clear maximum, and the best peak time moves earlier as the window becomes narrower. For the narrowest

window ($\beta = h^{-2}$), the best peak time is $t_h = 10.0$ h, which matches the time at which the xylitol pool is largest. For $\beta = 0.01\ h^{-2}$, the width used in the parent model ($\beta = 1/t_f$), the best peak time is $t_h = 17.0$ h and the harvest is *3.093* mM. the parent model palced the window at $t_h = 72$ h, which yields only *1.853* mM, so moving the window earlier increase the harvest by *66.9%* with no change in its width. The corresponding gains are *38.1%* for $\beta = 0.001\ \text{h}^{-2}$ ($t_h = 35.0$ h), 78.5% for $\beta = 0.1\ \text{h}^{-2}$ ($t_h = 10.5$ h) and *79.8%* dor $\beta = 1\ \text{h}^{-2}$ ($t_h = 10.0$ h).

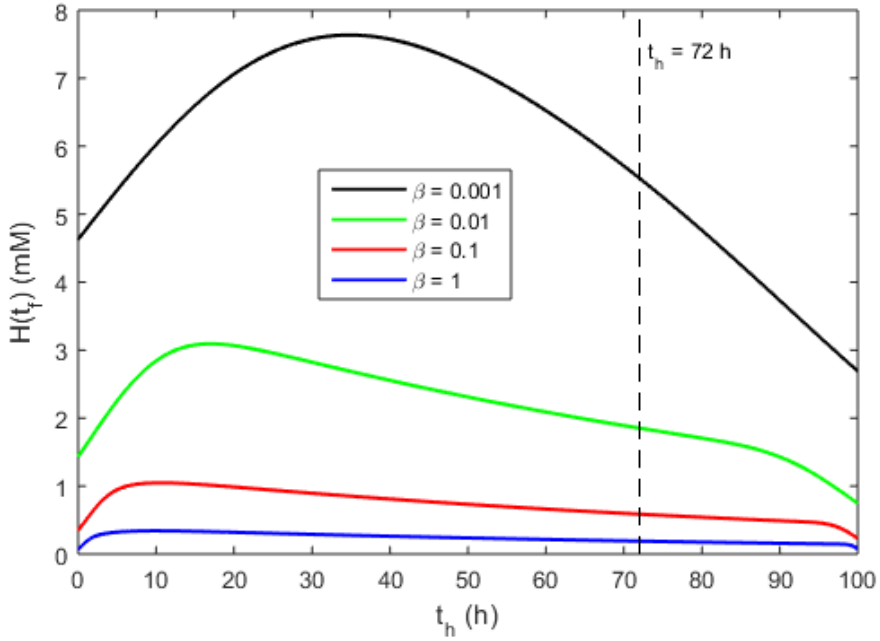


Figure 2. Cumulative harvest $H(t_f)$ as a function of the peak harvesting time t_h for four values of the window parameter β. The vertical line marks $t_h = 72$ h, the value used in the parent model.

When the cost of keeping the window open is included, the optimal schedule results from a balance between collecting more xylitol and shortening the operation. In the limiting case $c_\omega = 0$, the optimum lies on the lower boundary of β, as anticipated in Section 2.2, because a wider window always increases the harvest. For positive costs, the objective J has a single interior maximum, which is visible in the contour maps of Figure 3. The optimal schedules for three cost scenarios are summarized in Table 2. As c_ω increases from 0.05 to 0.15 mM h^{-1}, the optimal window narrows from 84.3 h to 19.2 h and its peak moves from 40.2 h to 17.8 h, approaching the time of maximum xylitol concentration. The harvest falls

accordingly, from 9.60 to 3.31 mM, and the efficiency falls from 15.18% to 5.24%. When c_ω exceeds about 0.19 mM h^{-1}, no schedule in Ω yields a positive net benefit. In this regime even the narrowest admissible window, which collects only 0.342 mM, costs more than it returns. The refined optima differed from the best grid points by less than 0.5 h in t_h and by less than one grid step in β. An independent coarse grid of 41 × 41 points gave optima within one coarse grid step of those from the fine grid.

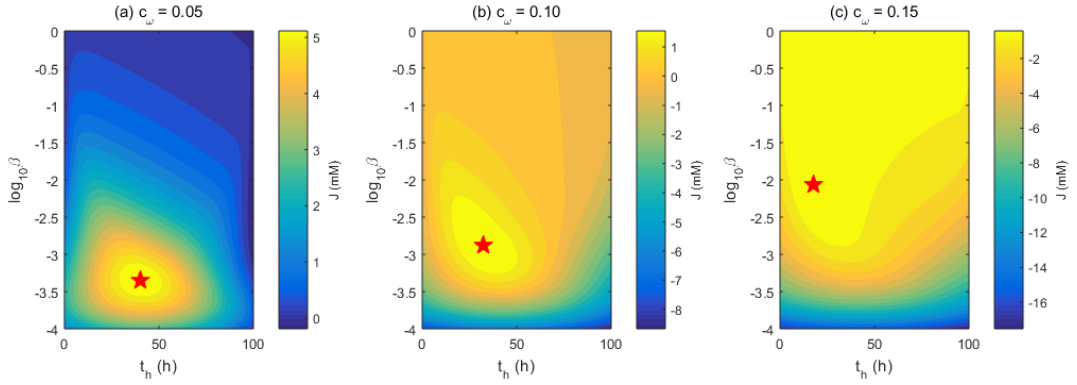


Figure 3. Contour maps of the objective $J(t_h, \beta)$ for (a) c_ω = 0.05, (b) c_ω = 0.10, and (c) c_ω = 0.15 $\mathrm{mM\ h^{-1}}$. The star marks the optimal schedule.

Table 2. Optimal harvesting schedules for three values of the window cost c_ω

c_ω ($mM\ h^{-1}$)	t_h^* (h)	β^* (h^{-2})	$W(\beta^*)$ (h)	$H(t_f)$ (mM)	J^* (mM)	η (%)
0.05	40.20	4.42×10^{-4}	84.29	9.596	5.381	15.18
0.10	32.18	1.31×10^{-3}	48.90	6.954	2.065	11.00
0.15	17.82	8.53×10^{-3}	19.19	3.315	0.437	5.24

The sensitivity of the optimal schedule was examined for the intermediate scenario $c_\omega = 0.05$ mM h^{-1}, and the results are summarized in Table 3. The optimal peak time proved robust: across all sixteen perturbations, t_h^* remained between 34.0 and 43.7 h, compared with 40.2 h at the nominal values. The amount harvested, by contrast, depended strongly on the parameters that govern the competition for xylitol. Reducing the activity of xylitol dehydrogenase (V_5) by 50% raised the efficiency from 15.18% to 27.99% and nearly

doubled the harvest, while increasing it by 50% lowered the efficiency to 9.70%. Changes in the harvesting rate constant δ_1 acted in the opposite direction, with the efficiency ranging from 6.49% at −50% to 22.12% at +50%. Both trends agree with Proposition 1. Changes in the xylose reductase capacity V_3 had almost no effect, with efficiencies between 15.03% and 15.23%. This is because V_3 greatly exceeds the xylose supply, so the reductase flux is set by the supply rather than by the enzyme. Changes in the release rate α altered the total amount harvested, because they change the total substrate supplied within 100 h, but they had only a modest effect on the efficiency, which stayed between 13.06% and 15.91%.

Table 3. Optimal schedule under one-at-a-time parameter perturbations ($c_\omega = 0.05$ mM h^{-1}).

Parameter	Change	t_h^* (h)	$W(\beta^*)$ (h)	$H(t_f)$ (mM)	η (%)
Nominal	–	40.20	84.28	9.596	15.18
V_3	−50%	41.32	83.81	9.498	15.03
	−25%	40.57	84.09	9.565	15.13
	+25%	39.97	84.41	9.613	15.21
	+50%	39.82	84.51	9.624	15.23
V_5	−50%	42.23	102.57	17.690	27.99
	−25%	41.20	92.80	12.615	19.96
	+25%	39.08	76.69	7.583	12.00
	+50%	37.74	69.62	6.131	9.70
δ_1	−50%	33.97	55.32	4.103	6.49
	−25%	38.78	74.27	7.058	11.17
	+25%	40.90	91.07	11.890	18.81
	+50%	41.33	96.05	13.985	22.12
α	−50%	43.75	66.56	5.139	13.06
	−25%	42.17	78.01	7.639	14.48
	+25%	38.18	87.88	11.139	15.61
	+50%	36.19	89.76	12.359	15.91

DISCUSSION

Reducing the fourteen-metabolite model to three variables turned out to cost nothing in accuracy while gaining a great deal in clarity. The closed-form equilibrium of the reduced model reproduces the steady-state concentrations of xylose, xylitol, and xylulose reported for the full model to five decimal places (Bani et al., 2025). This agreement is not a coincidence of parameter values. It follows from the structure of the network, in which glycolysis and the ethanol branch draw carbon from xylitol but return none to it. Because of this one-way flow, properties that could previously be checked only numerically can now be stated as theorems. Lemma 1 guarantees that the batch model never produces negative concentrations and that the intracellular pool cannot hold more material than was initially present plus what has been released from lignocellulose. Theorems 1–3 show that, under constant supply and continuous harvesting, the system has a single equilibrium that attracts every solution, so every fermentation run settles at the same xylitol level whatever its starting state. This level therefore serves as a natural benchmark against which any harvesting schedule can be judged.

The conditions of Theorem 1 have a direct biochemical reading: each enzyme must have a maximum capacity larger than the flux it is asked to carry. A less obvious consequence concerns harvesting itself. Without harvesting, a xylitol equilibrium exists only if xylitol dehydrogenase can oxidize the entire inflow. With harvesting, this restriction disappears, because harvesting provides a second outlet that keeps the xylitol pool bounded. Proposition 1 then describes how the two outlets compete. Stronger harvesting lowers the intracellular xylitol concentration but diverts a larger share of the inflow away from oxidation, whereas a more active xylitol dehydrogenase lowers both the concentration and the share that can be recovered. This picture is consistent with the metabolic control analysis of the parent model, in which xylitol dehydrogenase exerted the strongest negative control on xylitol concentration (Bani et al., 2025). It also agrees with experimental reports that weakening or removing this enzyme raises xylitol output, both in *Debaryomyces hansenii* (Pal et al., 2013) and in *Candida tropicalis* (Ko et al., 2006).

The numerical results put a size on this competition. Even when harvesting runs continuously at its maximum rate, only 19.47% of the precursor supplied over 100 h is recovered, which is close to the equilibrium fraction $\theta^* = 19.74\%$. The remaining four-fifths is oxidized to xylulose. This ceiling is set by the ratio between the harvesting rate constant and the oxidation capacity of the cell, not by the schedule. No choice of t_h and β

can push the efficiency above it. What a well-chosen schedule can do is approach the ceiling while keeping the harvesting operation short. At the intermediate cost $c_\omega = 0.05$ mM h^{-1}, the optimal schedule recovers 15.18% of the supply, about 78% of the maximum achievable, with an effective window of 84 h instead of the full run.

The most practically relevant finding concerns the timing of the window. The parent model placed the harvesting peak at $t_h = 72$ h with $\beta = 1/t_f$ (Bani et al., 2025). With the same window width, moving the peak to $t_h = 17$ h raised the harvest by 66.9%, from 1.853 to 3.093 mM, at no extra cost, since the width of the window, and hence the cost term in J, is unchanged. The reason is visible in Figure 1. The xylitol pool reaches its maximum at about 10 h and then declines slowly, because the lignocellulose-derived supply decays as $e^{-\alpha t}$. By 72 h this supply has fallen to about half of its initial value, and the pool has shrunk accordingly. A window centered late in the fermentation therefore spends most of its time collecting from a depleted pool. The time-scale separation between the slow decay of the supply ($1/\alpha = 100$ h) and the fast intracellular relaxation ($1/|\lambda_1| = 3.72$ h) explains why the pool follows the quasi-equilibrium so closely. It also explains why the best timing can be anticipated from the reference model alone: the harvest should be concentrated where the quasi-equilibrium $S_5^*\big(Q(t)\big)$ is highest, that is, early in the fermentation.

The dependence of the optimal peak time on the window width follows the same logic. A narrow window can be placed exactly at the maximum of the xylitol pool, which is why the best peak time approaches 10 h as β increases (Figure 2). A wide window cannot be centered there without wasting a large part of its span before the start of fermentation, where nothing can be collected. Its optimal center therefore shifts later, to about 35-40 h, so that the window covers as much of the declining but still substantial pool as possible. The cost coefficient c_ω decides where along this spectrum the optimum lies. As c_ω rises from 0.05 to 0.15 mM h^{-1}, the optimal window narrows from 84 to 19 h and moves from 40 to 18 h (Table 2), drifting toward the time of maximum xylitol concentration. Above $c_\omega \approx 0.19$ mM h^{-1}, no schedule within the admissible range yields a positive net benefit, which marks the point at which harvesting from this system is no longer worthwhile. Because the actual cost of a harvesting operation depends on the separation technology used, these results are best read as a family of schedules indexed by c_ω rather than as a single prescription.

The sensitivity analysis shows that the optimal timing is a robust property of the system, while the amount harvested is not. Across all sixteen perturbations, the optimal peak time stayed between 34 and 44 h (Table 3). A practitioner can therefore choose the timing with some confidence even when the kinetic parameters are uncertain. The amount harvested, by contrast, responded strongly to the two parameters that govern the competition for xylitol. Halving the activity of xylitol dehydrogenase raised the efficiency from 15.18% to 27.99%, and halving the harvesting rate constant lowered it to 6.49%. These results suggest that schedule optimization and enzyme-level intervention are complementary rather than competing strategies. Scheduling extracts the most from a given strain, and reducing xylitol dehydrogenase activity raises the ceiling within which scheduling operates. The capacity of xylose reductase, on the other hand, had almost no influence on the outcome. Under the supply conditions considered here, this enzyme works far below its maximum rate, so the flux into the xylitol pool is set by the release of xylose from lignocellulose rather than by the enzyme itself. Changes in the release rate α altered the total amount harvested but had only a modest effect on efficiency, since they change how much substrate arrives within the fermentation horizon rather than how it is divided once it arrives.

Several limitations should be kept in mind when interpreting these results. The kinetic parameters are inherited from the parent model, where several of them were taken from enzyme studies in organisms other than *D. hansenii*. The quantitative values reported here, especially the harvest amounts, should therefore be read as indicative, although the robustness of the optimal timing gives some reassurance about the qualitative conclusions. The harvesting function is phenomenological. It describes how intensely and when xylitol is removed, but not the separation technology that would achieve this, and the linear cost in window width is a simplification of real operating costs. The reduced model also treats xylitol removal as acting directly on the intracellular pool and does not include biomass growth, which is known to accompany xylitol production in this system (Bani et al., 2026). Finally, the results have not yet been tested experimentally. Natural extensions of this work include coupling the reduced metabolic model with an unstructured biomass model, allowing more than one harvesting window, treating the harvesting intensity as a time-varying control within an optimal control framework, and testing the predicted advantage of early harvesting in batch fermentation of OPEFB hydrolysate.

CONCLUSION

This study reduced the fourteen-metabolite model of *Debaryomyces hansenii* to a three-dimensional cascade of xylose, xylitol, and xylulose, and used it to determine when and for how long xylitol should be harvested. The reduced model reproduces the steady state of the full model exactly. For its reference version, we proved that solutions remain positive and bounded, that a unique positive equilibrium exists whenever harvesting is active, and that this equilibrium is globally asymptotically stable. We also showed analytically that harvesting and xylitol dehydrogenase compete for the same pool, with stronger harvesting diverting a larger share of the inflow away from oxidation.

The numerical results showed that timing matters more than previously assumed. With the window width used in the earlier model, moving the harvesting peak from 72 h to about 17 h increased the harvested xylitol by 66.9%, because the xylitol pool is largest early in the fermentation and declines as the lignocellulose-derived supply decays. When a cost proportional to the window width is included, the optimal window becomes narrower and earlier as the cost rises, and the optimal peak time remains between 34 and 44 h under all parameter perturbations considered. Even continuous harvesting, however, recovers less than 20% of the supplied precursor, because most xylitol is oxidized by xylitol dehydrogenase. Optimizing the harvesting schedule and reducing xylitol dehydrogenase activity should therefore be viewed as complementary strategies. Future work should couple the reduced model with biomass growth, consider time-varying harvesting through optimal control, and test the predicted benefit of early harvesting experimentally.

REFERENCES

Bani, A., Kasbawati, Toaha, S., Mardawati, E., Gozan, M., Nurhamiyah, Y., & Chen, B. (2026). Comparing unstructured kinetic growth models of *Debaryomyces hansenii* in xylitol production from oil palm empty fruit bunch hydrolysis. *Jambura Journal of Biomathematics, 7*(3), 559–575. https://doi.org/10.37905/jjbm.v7i3.34

Bani, A., Kasbawati, Toaha, S., Mardawati, E., Suhartini, S., Natsir, H., & Aris, N. (2026). Kinetic analysis of central metabolic regulation in *Debaryomyces hansenii* for enhanced xylitol and ethanol production from oil palm empty fruit bunches. *Chemical Engineering Communications, 213*(4), 744–768. https://doi.org/10.1080/00986445.2025.2578831

Biswas, D., Datt, M., Aggarwal, M., & Mondal, A. K. (2013). Molecular cloning, characterization, and engineering of xylitol dehydrogenase from *Debaryomyces hansenii*. *Applied Microbiology and Biotechnology, 97*(4), 1613–1623. https://doi.org/10.1007/s00253-012-4020-5

Clark, C. W. (2010). *Mathematical bioeconomics: The mathematics of conservation* (3rd ed.). Wiley. https://www.wiley-vch.de/en/areas-interest/mathematics-statistics/mathematics-16ma/applied-mathematics-16ma2/computational-biology-16ma23/mathematical-bioeconomics-978-0-470-37299-9

Feng, J., Techapun, C., Phimolsiripol, Y., Rachtanapun, P., Phongthai, S., Khemacheewakul, J., Taesuwan, S., Porninta, K., Htike, S. L., Mahakuntha, C., Sommanee, S., Nunta, R., Kumar, A., & Leksawasdi, N. (2024). Co-substrate model development and validation on pure sugars and corncob hemicellulosic hydrolysate for xylitol production. *Scientific Reports, 14*(1), Article 25928. https://doi.org/10.1038/s41598-024-77462-y

Gasmi Benahmed, A., Gasmi, A., Arshad, M., Shanaida, M., Lysiuk, R., Peana, M., Pshyk-Titko, I., Adamiv, S., Shanaida, Y., & Bjørklund, G. (2020). Health benefits of xylitol. *Applied Microbiology and Biotechnology, 104*(17), 7225–7237. https://doi.org/10.1007/s00253-020-10708-7

International Diabetes Federation. (2025). *IDF diabetes atlas* (11th ed.). https://diabetesatlas.org

Kasbawati, Kalondeng, A., Aris, N., Erawaty, N., & Azis, M. I. (2018). A kinetic modelling of enzyme inhibitions in the central metabolism of yeast cells. *Journal of Physics: Conference Series, 979*(1), Article 012066. https://doi.org/10.1088/1742-6596/979/1/012066

Kasbawati, Kalondeng, A., & Sulfahri. (2020). A numerical study of the sensitivity of ethanol flux to the existence of co-factors in the central metabolism of a yeast cell using multi-substrate enzymes kinetic modelling. *Biotechnology & Biotechnological Equipment, 34*(1), 375–383. https://doi.org/10.1080/13102818.2020.1758593

Kasbawati, K., Mardawati, E., Samsir, R., Suhartini, S., & Kalondeng, A. (2022). An appropriate unstructured kinetic model describing the batch fermentation growth of *Debaryomyces hansenii* for xylitol production using hydrolysis of oil palm empty fruit bunch. *Biotechnology & Biotechnological Equipment, 36*(1), 462–471. https://doi.org/10.1080/13102818.2022.2098816

Ko, B. S., Kim, J., & Kim, J. H. (2006). Production of xylitol from D-xylose by a xylitol dehydrogenase gene-disrupted mutant of *Candida tropicalis*. *Applied and Environmental Microbiology, 72*(6), 4207–4213. https://doi.org/10.1128/AEM.02699-05

Manjarres-Pinzón, K., Barrios-Ziolo, L., Arias-Zabala, M., Correa-Londoño, G., & Rodríguez-Sandoval, E. (2021). Kinetic study and modeling of xylitol production using *Candida tropicalis* in different culture media using unstructured models. *Revista Facultad Nacional de Agronomía Medellín, 74*(2), 9583–9592. https://doi.org/10.15446/rfnam.v74n2.92270

Mardawati, E., Febrianti, E. A., Fitriana, H. N., Yuliana, T., Putriana, N. A., Suhartini, S., & Kasbawati. (2022). An integrated process for the xylitol and ethanol production from oil palm empty fruit bunch (OPEFB) using *Debaryomyces hansenii* and *Saccharomyces cerevisiae*. *Microorganisms, 10*(10), Article 2036. https://doi.org/10.3390/microorganisms10102036

Navarrete, C., Estrada, M., & Martínez, J. L. (2022). *Debaryomyces hansenii*: An old acquaintance for a fresh start in the era of the green biotechnology. *World Journal of Microbiology and Biotechnology, 38*(6), Article 99. https://doi.org/10.1007/s11274-022-03280-x

Pal, S., Choudhary, V., Kumar, A., Biswas, D., Mondal, A. K., & Sahoo, D. K. (2013). Studies on xylitol production by metabolic pathway engineered *Debaryomyces hansenii*. *Bioresource Technology, 147*, 449–455. https://doi.org/10.1016/j.biortech.2013.08.065

Perko, L. (2001). *Differential equations and dynamical systems* (3rd ed.). Springer. https://doi.org/10.1007/978-1-4613-0003-8

Segel, L. A., & Slemrod, M. (1989). The quasi-steady-state assumption: A case study in perturbation. *SIAM Review, 31*(3), 446–477. https://doi.org/10.1137/1031091

Shampine, L. F., & Reichelt, M. W. (1997). The MATLAB ODE suite. *SIAM Journal on Scientific Computing, 18*(1), 1–22. https://doi.org/10.1137/S1064827594276424

Söderling, E., & Pienihäkkinen, K. (2025). Specific effects of xylitol chewing gum on mutans streptococci levels, plaque accumulation and caries occurrence: A systematic review. *BMC Oral Health, 25*(1), Article 1275. https://doi.org/10.1186/s12903-025-06602-1

Suhartini, S., Rohma, N. A., Mardawati, E., Kasbawati, Hidayat, N., & Melville, L. (2022). Biorefining of oil palm empty fruit bunches for bioethanol and xylitol production in Indonesia: A review. *Renewable and Sustainable Energy Reviews, 154*, Article 111817. https://doi.org/10.1016/j.rser.2021.111817

Thieme, H. R. (1992). Convergence results and a Poincaré–Bendixson trichotomy for asymptotically autonomous differential equations. *Journal of Mathematical Biology, 30*(7), 755–763. https://doi.org/10.1007/BF00173267

World Health Organization. (2022). *Global oral health status report: Towards universal health coverage for oral health by 2030*. https://www.who.int/publications/i/item/9789240061484